

Manuscript Title: Structure and Mechanism of Soybean ATP Sulfurylase and the Committed Step in Plant Sulfur Assimilation

Manuscript No: JBC/2013/540401 [R2]

Manuscript Type: Regular Paper

Date Submitted by the Author: 27 Feb 2014

Complete List of Authors: Jonathan Herrmann, Geoffrey E. Ravilious, Samuel E. McKinney, Corey S. Westfall, Soon Goo Lee, Patrycja Baraniecka, Marco Giovannetti, Stanislav Kopriva, Hari B. Krishnan, and Joseph M. Jez

Keywords: Enzyme mechanisms; Enzyme structure; Plant; Plant biochemistry; Protein structure

Structure and Mechanism of Soybean ATP Sulfurylase and the Committed Step in Plant Sulfur Assimilation

Jonathan Herrmann¹, Geoffrey E. Ravilious¹, Samuel E. McKinney¹, Corey S. Westfall¹, Soon Goo Lee¹, Patrycja Baraniecka², Marco Giovannetti^{2,3}, Stanislav Kopriva², Hari B. Krishnan⁴, Joseph M. Jez^{1,5}

From the ¹Department of Biology, Washington University, One Brookings Drive, Campus Box 1137, St. Louis, MO 63130; ²John Innes Centre, Norwich Research Park, Norwich, NR4 7UH, UK; ³Department of Life Sciences and Systems Biology, University of Torino, Viale Mattioli 25, I-10125, Torino, Italy; ⁴Plant Genetics Research Unit, USDA-Agricultural Research Service, University of Missouri, Columbia, MO 65211 USA

⁵To whom correspondence should be addressed: Joseph M. Jez, Department of Biology, Washington University, One Brookings Drive, Campus Box 1137, St. Louis, MO, 63130. Phone: 314-935-3376; E-mail: jjez@biology2.wustl.edu

Background: ATP sulfurylase catalyzes the energetically unfavorable formation of adenosine-5'-phosphosulfate in plant sulfur assimilation.

Results: Structural and kinetic analysis identifies key active site residues.

Conclusion: A reaction mechanism involving distortion of nucleotide conformation and stabilizing interactions is proposed.

Significance: These results provide the first molecular insights on a plant ATP sulfurylase and the committed step of plant sulfur assimilation.

Enzymes of the sulfur assimilation pathway are potential targets for improving nutrient content and environmental stress responses in plants. The committed step in this pathway is catalyzed by ATP sulfurylase, which synthesizes adenosine-5'-phosphosulfate (APS) from sulfate and ATP. To better understand the molecular basis of this energetically unfavorable reaction, the x-ray crystal structure of ATP sulfurylase isoform 1 from soybean (GmATPS) in complex with APS was determined. This structure revealed several highly conserved substrate-binding motifs in the active site and a distinct dimerization interface compared to other ATP sulfurylases, but similar to mammalian PAPS synthetase. Steady-state kinetic analysis of twenty GmATPS point mutants suggests a reaction mechanism in which nucleophilic attack by sulfate on the alpha-phosphate of ATP involves transition state stabilization by Arg248, Asn249, His255,

and Arg349. The structure and kinetic analysis suggest that ATP sulfurylase overcomes the energetic barrier of APS synthesis by distorting nucleotide structure and identifies critical residues for catalysis. Mutations that alter sulfate assimilation in Arabidopsis were mapped to the structure, which provides a molecular basis for understanding their effects on the sulfur assimilation pathway.

In plants, the uptake of sulfate and its assimilation provides an essential nutrient for the synthesis of a diverse set of metabolites, including cysteine, methionine, glutathione, iron-sulfur clusters, vitamin cofactors like biotin and thiamin, and multiple specialized metabolites such as glucosinolates (1-8). The central role of sulfur metabolism in plants and its integration with carbon and nitrogen metabolism and the biosynthesis of multiple specialized metabolites has led to efforts to understand this critical pathway for applications in nutritional enhancement for food and feed and for improved plant growth under environmental stresses (2, 9-15). Utilizing this environmental source of sulfur requires the enzymatic conversion of sulfate into chemical forms that are energetically favorable for reduction.

The first enzymatic step of plant sulfur assimilation is the non-reductive adenylation of sulfate by ATP sulfurylase (ATP:sulfate adenylyl transferase; EC 2.7.7.4), which catalyzes the formation of adenosine-5'-phosphosulfate (APS⁵) and inorganic pyrophosphate (PP_i) from sulfate and ATP (Fig. 1A) (16-17). Production of APS by ATP

sulfurylase, which is energetically unfavorable compared to the reverse reaction, is the committed step in plant sulfur assimilation and yields a high-energy phospho-sulfate bond that drives subsequent metabolic steps in the pathway (17-19). Reduction of APS to sulfite and then sulfide completes the sulfur assimilation pathway and supports cysteine biosynthesis (1, 4-8). APS can also be phosphorylated to 3'-phosphoadenosine-5'-phosphosulfate (PAPS) by APS kinase to provide a substrate for sulfonation reactions in plant primary and specialized metabolic pathways (20-27).

Multigene families encode ATP sulfurylase in the plant species examined to date, including *Arabidopsis thaliana* (thale cress), *Solanum tuberosum* (potato), *Brassica juncea* (Indian mustard), *Glycine max* (soybean), and *Camellia sinensis* (tea plant) (5, 18-19, 28-34). ATP sulfurylase isoforms are localized to different organelles with the chloroplast form associated with reductive sulfate assimilation and accounting for the highest portion of enzyme activity (35-36). For example, soybean contains four isoforms (GmATPS1-4), all of which are predicted to localize to the chloroplast (5). Expression of ATP sulfurylase is highest in young leaves, early stages of seed development, and the elongation zone of roots (19, 35-38). Traditionally, ATP sulfurylase has not been considered to be important for the control of flux through the sulfate assimilation pathway (39). The plastidic forms of ATP sulfurylase, however, are targeted by sulfur deprivation-inducible microRNA miR395, which increases translocation of sulfate from the roots to the shoots (40-41). Accordingly, disruption of the ATPS1 isoform of ATP sulfurylase in *Arabidopsis* results in increased accumulation of sulfate in the leaves (41). Thus, ATP sulfurylase contributes significantly to the control of plant sulfur metabolism; however, the molecular basis for its function remains poorly understood.

ATP sulfurylase is also important in a diverse range of organisms for sulfate activation and assimilation; however, the structural organization of the enzyme varies widely in both domain architecture and oligomerization (**Fig. 1B-C**). Some prokaryotic forms of ATP sulfurylase, including those from *Escherichia*

coli and *Pseudomonas syringae* are heterodimeric proteins comprised of a GTPase subunit and a catalytic ATP sulfurylase subunit (42). In other prokaryotes, including the thermophiles *Aquifex aeolicus* and *Thermus thermophilus*, the purple sulfur bacterium *Allochromatium vinosum*, and a bacterial symbiont of the vent tubeworm *Riftia pachyptila*, ATP sulfurylase functions either as a monofunctional homodimeric enzyme or a bifunctional homodimeric ATP sulfurylase/APS kinase, also known as PAPS synthetase (43-46). In fungi, such as *Saccharomyces cerevisiae* and *Penicillium chrysogenum*, ATP sulfurylase is a homohexamer in which each monomer contains an N-terminal ATP sulfurylase domain and a C-terminal APS kinase-like domain (47-49). The APS kinase-like domain can also function as an allosteric regulatory region in response to PAPS, as shown for the *P. chrysogenum* enzyme (50). The human PAPS synthetase operates as a homodimeric enzyme containing distinct ATP sulfurylase and APS kinase domains (51). Sequence comparisons and biochemical analyses suggest that the plant ATP sulfurylases are most closely related to the human ATP sulfurylase domain of PAPS synthetase and function as homodimeric proteins (19, 52). To date, no structural information is available for an ATP sulfurylase from any plant species to provide insight on how this enzyme functions as the committed step in plant sulfur assimilation.

EXPERIMENTAL PROCEDURES

Materials. All oligonucleotides used for site-directed mutagenesis were synthesized by Integrated DNA Technologies, Inc. Ni²⁺-nitrilotriacetic acid (NTA) was from Qiagen. The HiLoad 26/60 Superdex-200 FPLC column was purchased from GE Healthsciences. All other reagents were of ACS grade or better and were purchased from Sigma-Aldrich.

Protein expression, purification, and site-directed mutagenesis. The pET-28a-GmATPSΔ48 bacterial expression construct, which encodes *G. max* ATP sulfurylase isoform 1 (*Glyma10g38760a*) lacking the plastid localization sequence (residues 1-48) and with

an N-terminal hexahistidine tag, was previously described (19). *E. coli* Rosetta (DE3) transformed with pET-28a-GmATPS Δ 48 were grown at 37 °C in Terrific broth containing kanamycin (50 $\mu\text{g mL}^{-1}$) and chloramphenicol (34 $\mu\text{g mL}^{-1}$) until $A_{600\text{nm}} \sim 0.8$. Following induction of protein expression with 1 mM isopropyl 1-thio- β -D-galactopyranoside, the cultures were grown at 20 °C for 8 h. Cells were pelleted by centrifugation (10,000 x g) and resuspended in lysis buffer (50 mM Tris, pH 8.0, 500 mM NaCl, 20 mM imidazole, 10% glycerol, 1% Tween-20, and 1 mM β -mercaptoethanol). After sonication and centrifugation, the supernatant was passed over a Ni²⁺-NTA column equilibrated with lysis buffer. Unbound protein was eluted with wash buffer (lysis buffer without Tween-20) and His-tagged GmATPS was eluted with elution buffer (wash buffer containing 250 mM imidazole). Eluted protein was loaded onto a Superdex-200 FPLC column equilibrated with 25 mM HEPES (pH 7.5), 150 mM NaCl, and 1 mM D/L-dithiothreitol. Peak fractions were collected and concentrated to 12.5 mg mL⁻¹ using centrifugal concentrators (Amicon). Purity was assessed by SDS-PAGE. Purified protein was flash frozen in liquid nitrogen stored at -80 °C. Protein concentration was determined by the Bradford Method (Protein Assay; Bio-Rad) with BSA as standard. Site-directed mutants of GmATPS (F245L, F245A, Q246E, Q246N, Q246A, R248K, N249D, N249A, H252Q, H252N, H252A, H255Q, H255N, H255A, L258V, L258A, H333Q, H333N, H333A, and R349K) were generated using the QuikChange PCR method (Agilent) with expression and purification as described for wild-type GmATPS.

Protein crystallography. Crystals of GmATPS in complex with APS were grown at 4 °C in hanging drops with a 1:1 ratio of protein and crystallization buffer (0.1 M HEPES, pH 7.25, 18% PEG-8000, and 0.2 M NaCl) supplemented with 5 mM APS. For x-ray data collection, crystals were transferred to a cryoprotectant solution of mother liquor containing 20% ethylene glycol and flash-frozen in liquid nitrogen. X-ray diffraction data (0.5° oscillations; 360 images; 100 K) were collected

at SBC beamline 19-ID of the Advanced Photon Source at Argonne National Laboratory. The HKL3000 software suite was used to integrate, merge and scale diffraction intensities (53). The GmATPS structure was solved by molecular replacement using the structure of the ATP sulfurylase domain of human PAPS synthetase (residues 234-624; 59% sequence similarity; PDB: 1XNJ; 51) with ligands and water molecules removed as a search model. Molecular replacement was implemented with PHASER (54) and yielded an asymmetric unit with eight molecules with translation search Z-scores ranging from 18-23. The structural model of GmATPS was built in COOT (55) and refined using PHENIX (56). Initial model building and refinement used non-crystallographic symmetry restraints, which were released in later rounds. A translation-libration-screen (TLS) model, in which the each protein chain was treated as a single rigid group, was used throughout refinement. Iterative rounds of model building and refinement were continued until the R-factors converged to those reported in **Table 1**. Coordinates and structure factors for the GmATPS•APS complex were deposited in the Protein Data Bank (PDB: 4MAF).

Steady-state kinetic analysis of wild-type and mutant GmATPS. Steady-state kinetic analysis was performed using an enzyme-coupled spectrophotometric assay (52). Initial velocities for the reverse (i.e., ATP synthesis) reaction were measured using a Beckman DU800 UV/Vis spectrophotometer by observing the rate of change in absorbance of NADP⁺ at 340 nm ($\epsilon = 6270 \text{ M}^{-1} \text{ cm}^{-1}$) in 0.5 mL systems at 25 °C. Assays contained 50 mM Tris (pH 8.0), 5 mM MgCl₂, 1 mM NADP⁺, 1 mM glucose, 2 units of hexokinase, and 1 unit of glucose-6-phosphate dehydrogenase. Kinetic constants were determined using a matrix of varied substrate concentrations. Assays with wild-type GmATPS and the F245L, F245A, H252N, and H255Q mutants used 2.5-300 μM APS and 2.5-2,000 μM NaPP_i. For the Q246N and Q246A mutants, substrate concentrations were 2.5-500 μM APS and 5-2,000 μM NaPP_i. For the Q246E mutant, 25-5,000 μM APS and 5-

2,000 μM NaPP_i was used. Assays of the L258V, L258A, and R248K mutants used 2.5-300 μM APS and 20-5,000 μM NaPP_i . Substrate concentrations of 2-500 μM APS and 20-5,000 μM NaPP_i were used for assays of the N249A and R248K mutants. The N249D, H255A, and H333Q mutants were assayed using 1-200 μM APS and 2.5-2,000 μM NaPP_i . Assays to determine forward reaction (i.e., APS synthesis) kinetics of wild-type and mutant GmATPS contained 50 mM Tris (pH 8.0), 15 mM MgCl_2 , 100 mM NaCl, 0.2 mM NADH, 0.05 units of APS kinase, 20 units of pyruvate kinase, and 30 units of lactate dehydrogenase with varied ATP (50-10,000 μM) and Li_2SO_4 (50-10,000). Calculation of k_{cat} and K_m values used SigmaPlot (Systat Software) to fit data to the rate equation for an ordered bi bi reaction, $v/E = k_{\text{cat}}[A][B]/(K_m^A K_m^B + K_m^B[A] + K_m^A[B] + [A][B])$.

Substrate modeling. Molecular docking experiments were performed by Autodock vina (ver. 1.1.2) (57) with standard protocols. Computer docking of substrates into the GmATPS active site used a $30 \times 30 \times 30$ Å grid box with the level of exhaustiveness = 20. For modeling of the forward reaction, ATP and sulfate were manually modeled into the structure of GmATPS as a starting point. The position of sulfate was fixed based on the sulfate moiety in the GmATPS•APS complex structure. Docking of ATP yielded a calculated affinity of -8.6 kcal/mol with r.m.s.d. ranges of 1.35-2.90 Å. For the reverse reaction, the crystallographic position of APS in GmATPS was used and the initial placement of PP_i based on the crystal structure of yeast ATP sulfurylase in complex with APS and PP_i (48). Docking of PP_i into the structure yielded a calculated affinity of -4.8 kcal/mol with r.m.s.d. ranges of 0-0.44 Å.

Analysis of plant material. Arabidopsis accessions were grown for five weeks in controlled environment room under a short day 10-h-light/14-h-dark cycle at constant temperature of 22°C, 60% relative humidity, and light intensity of 160 $\mu\text{E s}^{-1}\text{m}^{-2}$. ATP sulfurylase activity was measured in leaf extracts as the APS and PP_i -dependent formation

of ATP and sulfate was determined by HPLC, as described in Kawashima et al. (41).

RESULTS

Overall three-dimensional structure of a plant ATP sulfurylase. Soybean ATP sulfurylase isoform 1 (GmATPS) was overexpressed in *E. coli* as an N-terminal His-tagged protein and purified using Ni^{2+} -affinity and size-exclusion chromatography, as previously described (19, 52). Purified GmATPS eluted from the gel-filtration column as a dimer of ~100 kDa formed from two 48 kDa monomers (19, 52).

The x-ray crystal structure of GmATPS was determined at 2.48 Å resolution by molecular replacement (**Table 1; Fig. 2**). Each monomer of GmATPS consists of two mixed α/β structural domains (**Fig. 2A**). The N-terminal domain (residues 48-211) is centered on an eight-stranded β -sheet ($\beta 1\text{a}-\beta 8\text{a}$) surrounded by four α -helices ($\alpha 1$, $\alpha 2$, $\alpha 4$, and $\alpha 6$). A second β -sheet ($\beta 1\text{b}-\beta 2\text{b}$) and two additional α -helices ($\alpha 3$ and $\alpha 5$) form most of the dimerization interface (**Fig. 2B**). A short loop (residues 212-226) connects the two halves of the monomer. The C-terminal domain (residues 227-447) is formed by a core β -sheet ($\beta 1\text{c}-\beta 5\text{c}$) and five α -helices ($\alpha 7-\alpha 11$) with a sub-domain consisting of a β -sheet ($\beta 1\text{d}-\beta 3\text{d}$) and two α -helices ($\alpha 12-\alpha 13$) positioned as a lid over the APS-binding site. One helix of the C-terminal domain ($\alpha 11$) also contributes to the dimer interface. The dimeric structure of GmATPS (**Fig. 2B**) positions the active site of each monomer in opposite orientations by a 2-fold rotation axis with respect to the dimer interface.

Structural comparison with ATP sulfurylases from other species. A search of the Protein Data Bank using DALI (58) showed that the overall fold of the GmATPS monomer was most similar to that of the ATP sulfurylase domain of human PAPS synthetase with a 0.9 Å root mean square deviation (r.m.s.d) for 390 aligned C α -atoms. This is consistent with the 59% amino sequence similarity between these two eukaryotic ATP sulfurylases (**Fig. 1B-C; Fig. 3**). The ATP sulfurylases from *T.*

thermophilus, *S. cerevisiae*, *P. chrysogenum*, *A. aeolicus*, and the *Riftia* symbiont, which share 26-29% amino acid sequence similarity with GmATPS, displayed larger structural variations of 1.6-2.7 Å r.m.s.d. over 360-390 aligned C α -atoms, although the overall fold was similar. No significant structural or sequence similarity was detected between GmATPS and the catalytic ATP sulfurylase subunit of the *P. syringae* enzyme.

Although the overall structure of the ATP sulfurylase monomer from various organisms is generally conserved, with the exception of the heterodimeric form of the enzyme, the oligomerization of the enzyme from different species is diverse (**Fig. 4**). As noted above, the dimer interface of GmATPS is formed by a β -sheet (β 1b- β 2b) and three α -helices (α 3, α 5, and α 11) (**Figs. 2B & 4**). This organization is also found in the ATP sulfurylase domain of the bifunctional human PAPS synthetase (**Fig. 4**). The APS kinase domain of the human enzyme is also dimeric with a flexible loop linking the two domains of each bifunctional monomer. Structural and sequence comparison of GmATPS with the *Riftia* symbiont and *T. thermophilus* ATP sulfurylases shows that major sequence variation in the features defining the dimerization region of the soybean enzyme (**Fig. 3**) leads to structural remodeling of the interface between monomers in the two bacterial proteins (**Fig. 4**). Interestingly, dimerization of the bifunctional *A. aeolicus* enzyme does not involve the ATP sulfurylase domains, but occurs through the APS kinase domain (**Fig. 4**). Similarly, the hexameric structure of the *S. cerevisiae* and *P. chrysogenum* ATP sulfurylases is also mediated through other regions of the monomer and not the catalytic domain (**Fig. 4**). Ultimately, the diverse sequence changes that have lead to varied oligomeric interaction features do not alter conserved regions of ATP sulfurylase necessary for catalysis (**Fig. 3**).

Active site structure of GmATPS. In the GmATPS structure, APS binds in the C-terminal domain of each monomer to clearly define the location of the active site (**Fig. 2**). Unambiguous electron density for APS was observed in each monomer of the asymmetric

unit (**Fig. 5A**). The ligand is bound in an enclosed cavity with a wide channel leading to the surface (**Fig. 5B**). The channel is positioned above the α -phosphate of APS and is lined with positively-charged residues, including Arg248, His252, His255, and Arg349 and provides a site for binding of the β - and γ -phosphates of ATP and PP_i. Residues from the β 1c- α 8 loop, α 10, and the N-terminal part of the β 4c- α 11 loop contribute to the active site and are highly conserved across the ATP sulfurylases from different organisms (**Fig. 3**). The enclosed active site suggests possible movement of the C-terminal sub-domain (residues 390-447; β 1d- β 3d and α 12- α 13) that forms a lid over the APS binding site to provide access of adenine nucleotides at the catalytic site. A recent crystal structure of the apoenzyme form of ATP sulfurylase from the purple sulfur bacterium *Allochromatium vinosum* reveals movement of α 12 to open the active site (46).

The GmATPS•APS complex provides a detailed view of interactions in the active site (**Fig. 5C**). The N1 and side-chain amine of the adenine ring form hydrogen bonds with the backbone nitrogen of Ala390 (2.9 Å) and the carbonyl of Ala390 (3.1 Å), respectively. In addition, the adenine ring makes van der Waals contacts with the side-chains of Leu258 and Arg349. The hydroxyl groups of the ribose hydrogen interact with the backbone nitrogen of Gly348 (3.1 Å). Extensive interactions between the phospho-sulfate mixed anhydride and active site residues are observed. Backbone nitrogens of Arg248 (3.1 Å) and Asn249 (2.6 Å) contact the phosphate group of APS. The side-chain amide of Gln246 (3.0 Å), the backbone nitrogen of Ala352 (2.9 Å), and the basic guanidyl group of Arg248 (3.1 Å) anchor the sulfate-derived portion of APS in the active site. Phe245, Val247, Met322, and His333 contribute additional van der Waals contacts. The side-chains of His252, His255, and Arg349 are positioned in the cavity leading to the surface of the protein and likely contribute to binding the β - and γ -phosphates of ATP in the forward reaction and PP_i in the reverse reaction. With the exceptions of Ala352 and Ala390, the amino acids forming the catalytic site of GmATPS are

invariant across the structurally characterized ATP sulfurylases (**Fig. 3**).

Functional analysis of GmATPS active site mutants. Based on the crystal structure of the GmATPS•APS complex, twenty point mutants of GmATPS (F245L, F245A, Q246E, Q246N, Q246A, R248K, N249D, N249A, H252Q, H252N, H252A, H255Q, H255N, H255A, L258V, L258A, H333Q, H333N, H333A, and R349K) were generated to introduce changes in active site residues for subsequent steady-state kinetic analysis. The H252Q, H252A, H255N, H333N, and H333A mutants led to expression of insoluble protein in *E. coli*; however, all other GmATPS were soluble and purified as dimeric enzymes.

Assays of the APS synthesis reaction catalyzed by wild-type and mutant GmATPS showed that only the F245L, Q246N, Q246A and H333Q mutants retained sufficient activity for determination of kinetic constants (**Table 2**). In general, the F245L, Q246N, Q246A and H333Q mutants displayed modest changes in turnover rates and/or K_m values compared to wild-type. Additional steady-state kinetic analysis of point mutants in the active site used the reverse (i.e., ATP synthesis) reaction because it provides better assay sensitivity compared to the forward reaction (**Table 3**).

Mutations in residues making van der Waals contacts with APS (i.e., F245L, F245A, L258V, L258A, and H333Q) generally led to modest less than 5-fold changes in steady-state kinetic parameters with either APS or sodium pyrophosphate. An 8-fold increase in K_m for pyrophosphate was observed with the L258A mutant.

Changes to amino acids in the sulfate- and phosphate-binding pockets of the active site introduced varied effects. The Q246A and Q246N mutants displayed k_{cat} and K_m values comparable to wild-type enzyme, but introduction of a negatively-charged side-chain in the Q246E mutant resulted in a 28-fold decrease in catalytic efficiency (k_{cat}/K_m) for APS and a modest 4-fold decrease in k_{cat}/K_m for PP_i . Replacement of Arg248 with a lysine altered catalytic efficiency with APS less than 2-fold, but decreased the k_{cat}/K_m for PP_i by 15-fold. The N249A mutant affected the kinetic parameters of

PP_i with a 22-fold decrease in catalytic efficiency that resulted largely from an increased K_m for this substrate. The kinetic parameters of this mutant should be considered as estimates as a saturating concentration of $NaPP_i$ could not be used. Substitution of an aspartate at this position (N249D) led to a 308-fold decrease in k_{cat} and 59- and 466-fold decreases in k_{cat}/K_m for APS and PP_i , respectively.

Mutations in the putative PP_i -binding site also altered the kinetic parameters of GmATPS. The R349K mutant reduced the turnover rate by 10-fold and lowered the k_{cat}/K_m values for APS and PP_i by 10- and 127-fold, respectively. Although changes of His252 largely resulted in insoluble protein, as noted above, the H252N mutant exhibited kinetic parameters comparable to wild-type protein. Substitution of His255 with a glutamine also did not dramatically alter the kinetic properties of the mutant enzyme; however, the H255A mutant displayed a 15-fold effect on k_{cat} for both substrates and a 10-fold decrease in catalytic efficiency for PP_i .

Analysis of sequence variation, sulfate content, and ATP sulfurylase activity in Arabidopsis ATPS1 haplotypes. In *A. thaliana*, alteration of ATP sulfurylase expression leads to increased sulfate accumulation (40-41; 59). To investigate the effect of sequence variation in *Arabidopsis* ATPS1 haplotypes, the ATP sulfurylase activity and sulfate levels of selected representative accessions were analyzed (**Table 4**). Haplotype data for ATPS1 was derived from the Arabidopsis 1001 Genomes database (<http://signal.salk.edu/atg1001/3.0/gebrowser.php>) (60). ATP sulfurylase activity and sulfate levels were determined in leaves of accessions representative of each haplotype. For comparison, ATP sulfurylase activity and sulfate content were measured in *A. thaliana* Col-0 and *atps1* mutant grown at the same conditions. High variation in sulfate levels was observed, with some accessions, such as Dog-4, Vie-0, Goettingen-7, Ciste-2, Naes-2, and Kulturen, accumulating higher sulfate levels than Col-0 (**Table 4**). These accessions were thus similar in the high sulfate phenotype to *atps1*, although the accumulation was not as pronounced as in the mutants (**Table 4**).

DISCUSSION

ATP sulfurylase plays a critical role in the plant sulfur assimilation pathway by catalyzing its first committed step via the energetically unfavorable formation of APS (**Fig. 1A**). The resulting phospho-sulfate bond of APS contains twice the energy of the pyrophosphate linkage in ATP and provides the driving force for reductive sulfur assimilation in plants (16-17). To overcome this energetic barrier, plants use a range of metabolic strategies, including the rapid use of the products of ATP sulfurylase in subsequent reactions catalyzed by APS reductase for sulfur assimilation, APS kinase for the generation of PAPS as a sulfonation donor molecule, and removal of PP_i by pyrophosphatase (5-8, 19-22, 25, 61-62).

The diversity in both sequence and structure of ATP sulfurylase (**Figs. 1B-C, 3, & 4**) reflects the distant origins of sulfur metabolism in different organisms and its various metabolic purposes. For the reductive assimilation of sulfate from the environment, ATP sulfurylase provides activated molecules for the synthesis of amino acids and specialized metabolites. In some microorganisms, sulfate reduction and sulfide oxidation function in a dissimilatory process to support consumption of sulfate and sulfur compounds for electron transfer processes. Multiple studies of ATP sulfurylases from a variety of organisms highlight the conservation of the catalytic core of the enzyme in terms of both three-dimensional structure and active site residues despite the distant evolutionary relationships of these organisms. Given the retention of the three-dimensional structure of ATP sulfurylase, this activity likely evolved before divergence of the different branches on the tree-of-life (46). These studies also reveal the versatility of the ATP sulfurylase fold as sequence variations that alter the oligomerization interface lead to a range of architectures for this enzyme (**Figs. 3 & 4**) (43-45, 47-51).

Interestingly, genome analysis of the sulfate utilization genes in the major eukaryotic and prokaryotic lineages suggest complex origins of the enzymes in these pathways and that crystallographic and biochemical studies of ATP sulfurylase have only examined a few of the

possible ways to organize the initial steps of sulfur assimilation (3, 62). For example, bioinformatic studies have identified independent and fused forms of ATP sulfurylase, APS kinase, sulfotransferase, pyrophosphatase, APS reductase, and related regulatory domains in various organisms (3, 62). Phylogenetic analysis of sulfur pathway genes by Bradley et al. (62) suggests a model for the evolution of these enzymes that invokes an ancestral gene fusion of ATP sulfurylase and APS kinase in two possible orientations to provide a common evolutionary origin for ATP sulfurylase/APS kinase fusion and another origin for APS kinase/ATP sulfurylase fusion. Subsequent gene fission, gene loss, and lateral gene transfer led to the variety of molecular architectures for these enzymes.

It remains unclear if ATP sulfurylase architecture is related to the evolution of regulatory structural features. In the heterodimeric enzymes from *E. coli* and *P. syringae*, the GTPase subunit allosterically activates the catalytic ATP sulfurylase subunit (42); however, this mechanism seems specialized for certain prokaryotes. Of the ATP sulfurylases structurally-related to GmATPS (**Figs. 1 & 4**), only the *P. chrysogenum* enzyme has a demonstrated allosteric regulatory mechanism involving PAPS (49-50). The observed structural transition in response to PAPS levels provides for control of sulfate activation in *P. chrysogenum*, but does not appear to be a widely-used regulatory feature in other organisms. However, localized structural changes are important for substrate binding.

The enclosed active site of GmATPS (**Figs. 2 & 5B**) suggests that conformational changes occur to accommodate substrate access and product exit from the enzyme. Substrate recognition in ATP sulfurylases requires several regions around the active site for nucleotide and sulfate/PP_i binding and reduced solvent access (**Fig. 5C**) (43-45, 47-50). Localized structural changes were observed in the apoenzyme structure of the *Riftia* symbiont ATP sulfurylase, which showed residues corresponding to the β 2c- α 9 loop of GmATPS rotated away from the active site (43). The recently determined crystal structure of an apoenzyme form of the enzyme

from the purple sulfur bacterium *Allochromatium vinosum* reveals movement of α 12 to open the active site (46).

Although multiple ATP sulfurylases from different organisms have been crystallized and structurally characterized, functional analysis of these enzymes is limited to the two histidines near the active site that correspond to His252 and His255 of GmATPS (63-64). The HXXH motif was originally identified in nucleotidylyl transferases and type I amino-acyl transferases (65-67). In these enzymes, the conserved histidines are directly involved in cleavage of the α/β -phosphate bond. Mutagenesis of the HXXH motif in the ATP sulfurylase domain of human and mouse PAPS synthetase lead to reduced specific activity (63-64), but more detailed steady-state kinetic analysis of the effect on function was not performed. To date, no structure-function analysis of other active site residues of an ATP sulfurylase from any other species has been reported.

The structure of GmATPS in complex with APS provides detailed information on the active site and protein-ligand interactions (**Figs. 2 & 5**). Mutagenesis of GmATPS identifies key active site residues and examines their contributions to catalysis and substrate recognition (**Tables 2-3**). Substitutions in residues making surface contacts with APS (including Phe245, Leu258, and His333) result in minor changes in steady-state kinetic parameters. Mutations in the His252 and His255 (i.e., the HXXH-motif) of GmATPS suggests that the role of the first histidine may be structural, as some changes in this residue led to production of insoluble protein. Removal of the His255 side-chain in the H255A mutant shows a 15-fold reduction in turnover rate, which suggests the loss of a stabilizing hydrogen bond interaction in catalysis. These results are consistent with the proposal that these two conserved histidines are not directly involved in cleavage of the α/β -phosphodiester bond.

Mutation of Gln246, which hydrogen bonds with the sulfate group of APS, suggests that this residue is not critical for substrate interaction; however, introduction of a negative charge at this position (i.e., Q246E) weakens affinity for APS, as suggested by the 28-fold decrease in

k_{cat}/K_m . This likely results from charge repulsion in the APS binding site of this mutant. Subtle alteration in Arg248 to a lysine retains interaction with APS, but reduces k_{cat}/K_m for PP_i by 15-fold suggesting the loss of interaction with this group during catalysis. Of the GmATPS active site residues, Asn249 and Arg349 are critical for efficient catalysis. The N249A mutation resulted in a 22-fold decrease in catalytic efficiency with PP_i . Introduction of a negative charge (N249D) caused the largest fold changes in steady-state kinetic parameters of any mutation in the GmATPS active site for both substrates. Substitution of Arg349 with a lysine reduced turnover rate by up to 10-fold, but decreased the k_{cat}/K_m for PP_i by 128-fold.

Molecular docking of the forward reaction substrates ATP and sulfate (**Fig. 6A**) and the reverse reaction substrates APS and PP_i (**Fig. 6B**) in the GmATPS active site suggests that Asn249 and Arg349, which are on opposite sides of the active site, have potential roles in catalysis. For the forward reaction, the positions of the sulfate ion and the adenine and ribose groups of ATP were initially placed based on the GmATPS•APS complex. Docking of ATP places the phosphate groups into the opening that leads to solvent from the active site and interactions with Arg248, Asn249, His255, and Arg349 (**Fig. 6A**). The distorted U-shape of the ATP is similar to the conformation observed in nucleotidylyl transferases (65). This conformation situates the α -phosphate group of ATP for in-line nucleophilic attack by the sulfate group and subsequent formation of APS and release of PP_i . Distortion of the phosphate backbone energetically contributes to overcoming the reaction barrier and leads to formation of the high energy mixed anhydride bond of APS (68). For the energetically favorable reverse reaction (i.e., ATP synthesis), positioning of PP_i by interactions with Asn249, His255, and Arg349 allows for facile nucleophilic attack on the α -phosphate of APS (**Fig. 6B**). Modeling of substrates in the GmATPS structure supports the proposed roles for various active site residues. Overall, both the forward and reverse reactions are substitution mechanisms that rely on reactive groups in close contact with both substrates to

provide protein-ligand interactions that stabilize a pentavalent transition state and enhance reaction rates. Because the active site residues of GmATPS are invariant across the ATP sulfurylases from other organisms, the functional role of these amino acids is likely conserved.

The structural and functional analyses presented here provide the first molecular insights on a plant ATP sulfurylase and the committed step of plant sulfur assimilation. Each method identified several amino acid residues important for the enzyme activity located in the active center. To identify further residues that might be important for ATP sulfurylase function we exploited natural variation in *A. thaliana* accessions. The ATP sulfurylase activity in the *atps1* mutant is decreased by ca. 50%, which together with the strong sulfate phenotype suggests that in Arabidopsis ATPS1 is the major isoform (4). Thus, sequence variation in ATPS1 that alter protein stability and/or proper folding may affect sulfate levels in Arabidopsis leaves.

Examination of ATPS1 sequences in the Arabidopsis 1001 Genomes database (<http://signal.salk.edu/atg1001/3.0/gebrowser.php>) identified numerous accessions with altered amino acid sequence of the protein (**Table 4**) (60). Sulfate levels in leaves of accessions representative of most haplotypes were determined. Some accessions (Dog-4, Vie-0, Goettingen-7, Ciste-2, Naes-2, and Kulturen) contained higher sulfate levels than Col-0. These accessions were thus similar in the high sulfate phenotype to *atps1*, although the accumulation has not been as pronounced as in the mutants (**Table 4**). Because the differences in sulfate levels may not be connected with the variation in ATPS1, we determined total ATP sulfurylase activity in the accessions. In all the accessions except Naes-2, activity was not different from Col-0 or even higher. The resulting effects of Naes-2 suggest that the amino acid variation in the ATPS1 protein (i.e., G342D) may affect protein function.

The 79% amino acid sequence identity between GmATPS and AtATPS1 allows for the mapping of Arabidopsis haplotype variations onto the GmATPS structure (**Fig. 7**). No variations were observed in any residues linked

to active site structure. Three mutations (S9R, V43N, and G56S) are in the localization sequence and/or region corresponding to the disordered region of GmATPS and were not mapped to the structural model of AtATPS1. Multiple changes (A144T, T150S, N160K, N202S, E312V, and A337S) occur in residues found in loops between secondary structure features (**Fig. 7**). Because mutations in loop regions are often tolerated, these changes would be predicted not to alter ATP sulfurylase function.

In comparison, changes in amino acids found in the dimer interface may affect activity by altering oligomerization and/or disrupting proper protein folding. Three variants (L122V, E169A, and K372R) across the Arabidopsis accessions are found in the dimer interface. Leu122 of AtATPS1 is invariant in the β 1b strand of all ATP sulfurylases from different organisms (**Fig. 3**). The L122V change may affect protein stability and/or folding. Similarly, the E169A mutation leads to removal of a charged side-chain at the start of α 7 where conservation of an acidic residue at this position occurs (**Fig. 3**). This mutation may alter stability and/or structure of AtATPS1. The K372R variant likely does not alter enzyme activity, as an arginine is found at this position in other plant homologs. Based on the positions of the T198A, V316F, and G342D changes in these residues, all of which alter the size and/or properties of the side-chain, may negatively impact protein structure because these residues are internally packed. Indeed, the Naes-2 accession with the G342D variant of ATPS1 shows decreased total ATP sulfurylase activity and sulfate accumulation. Mapping of Arabidopsis haplotype mutations onto the GmATPS crystal structure provides a molecular basis for understanding their effects on sulfur metabolism and for dissecting the natural variation in ATP sulfurylase and the structure/function relationship of the enzyme isoforms.

REFERENCES

1. Leustek, T., Martin, M.N., Bick, J.A., and Davies, J.P. (2000) Pathways and regulation of sulfur metabolism revealed through molecular and genetic studies. *Annu. Rev. Plant Physiol. Plant Mol. Biol.* 51, 141-165
2. Krishnan, H.B. (2005) Engineering soybean for enhanced sulfur amino acid content. *Crop Sci.* 45, 454-461
3. Patron, N.J., Durnford, D.G., and Kopriva, S. (2008) Sulfate assimilation in eukaryotes: fusions, relocations, and lateral transfers. *BMC Evol. Biol.* 8, 39
4. Yi, H., Galant, A., Ravilious, G.E., Preuss, M.L., and Jez, J.M. (2010) Sensing sulfur conditions: simple to complex protein regulatory mechanisms in plant thiol metabolism. *Mol. Plant* 3, 269-279
5. Yi, H., Ravilious, G.E., Galant, A., Krishnan, H.B., and Jez, J.M. (2010) From sulfur to homogluthathione: thiol metabolism in soybean. *Amino Acids* 39, 963-978
6. Takahashi, H., Kopriva, S., Giordano, M., Saito, K., and Hell, R. (2011) Sulfur assimilation in photosynthetic organisms: molecular functions and regulations of transporters and assimilatory enzymes. *Annu. Rev. Plant Biol.* 62, 157-184
7. Kopriva, S., Mugford, S.G., Baraniecka, P., Lee, B.R., Matthewman, C.A., and Koprivova, A. (2012) Control of sulfur partitioning between primary and secondary metabolism in Arabidopsis. *Front. Plant Sci.* 3, 163.
8. Ravilious, G.E. and Jez, J.M. (2012) Structural biology of plant sulfur metabolism: from assimilation to biosynthesis. *Nat. Prod. Rep.* 29, 1138-1152
9. Höfgen, R., Kreft, O., Willmitzer, L., and Hesse, H. (2001) Manipulation of thiol contents in plants. *Amino Acids* 20, 291-299
10. Hawkesford, M.J. and De Kok, L.J. (2006) Managing sulphur metabolism in plants. *Plant Cell Environ.* 29, 382-395
11. White, P.J. and Brown, P.H. (2010) Plant nutrition for sustainable development and global health. *Ann. Bot.* 105, 1073-1080
12. Ohkama-Ohtsu, N. and Wasaki, J. (2010) Recent progress in plant nutrition research: cross-talk between nutrients, plant physiology and soil microorganisms. *Plant Cell Physiol.* 51, 1255-1264
13. Shin, R., Jez, J.M., Basra, A., Zhang, B., and Schachtman, D.P. (2011) 14-3-3 Proteins fine-tune plant nutrient metabolism. *FEBS Lett* 585, 143-147
14. Aharoni, A. and Galili, G. (2011) Metabolic engineering of the plant primary-secondary metabolism interface. *Curr. Opin. Biotechnol.* 22, 239-244
15. Chan, K.X., Wirtz, M., Phua, S.Y., Estavillo, G.M., and Pogson, B.J. (2013) Balancing metabolites in drought: the sulfur assimilation conundrum. *Trends Plant Sci.* 18, 18-29
16. Asahi, T. (1964) Sulfur metabolism in higher plants: IV. mechanism of sulfate reduction in chloroplasts. *Biochim. Biophys. Acta* 82, 58-66
17. Osslund, T., Chandler, C., and Segel, I. (1982) ATP sulfurylase from higher plants: purification and preliminary kinetics studies of the cabbage leaf enzyme. *Plant Physiol.* 70, 39-45
18. Murillo, M. and Leustek, T. (1995) Adenosine-5'-triphosphate sulfurylase from *Arabidopsis thaliana* and *Escherichia coli* are functional equivalent but structurally and kinetically divergent: nucleotide sequence of two adenosine-5'-triphosphate sulfurylase cDNAs from *Arabidopsis thaliana* and analysis of a recombinant enzyme. *Arch. Biochem. Biophys.* 323, 195-204
19. Phartiyal, P., Kim, W.S., Cahoon, R.E., Jez, J.M., and Krishnan, H.B. (2006) Soybean ATP sulfurylase, a homodimeric enzyme involved in sulfur assimilation, is abundantly expressed in roots and induced by cold treatment. *Arch. Biochem. Biophys.* 450, 20-29
20. Klein, M. and Papenbrock, J. (2004) The multi-protein family of Arabidopsis sulphotransferases and their relatives in other plant species. *J. Exp. Bot.* 55, 1809-1820
21. Mugford, S.G., Yoshimoto, N., Reichelt, M., Wirtz, M., Hill, L., Mugford, S.T., Nakazato, Y., Noji, M., Takahashi, H., Kramell, R., Gigolashvili, T., Flügge, U.I., Wasternack, C., Gershenzon, J., Hell, R., Saito, K., and Kopriva, S. (2009) Disruption of adenosine-5'-phosphosulfate kinase in Arabidopsis reduces levels of sulfated secondary metabolites. *Plant Cell* 21, 910-927

22. Mugford, S.G., Matthewman, C.A., Hill, L., and Kopriva, S. (2010) Adenosine-5'-phosphosulfate kinase is essential for *Arabidopsis* viability. *FEBS Lett.* 584, 119-123
23. Yatusевич, R., Mugford, S.G., Matthewman, C., Gigolashvili, T., Frerigmann, H., Delaney, S., Koprivova, A., Flügge, U.I., and Kopriva, S. (2010) Genes of primary sulfate assimilation are part of the glucosinolate biosynthetic network in *Arabidopsis thaliana*. *Plant J.* 62, 1-11
24. Ravilious, G.E., Nguyen, A., Francois, J.A., and Jez, J.M. (2012) Structural basis and evolution of redox regulation in plant adenosine-5'-phosphosulfate kinase. *Proc. Natl. Acad. Sci. USA* 109, 309-314
25. Ravilious, G.E. and Jez, J.M. (2012) Nucleotide binding site communication in *Arabidopsis thaliana* adenosine 5'-phosphosulfate kinase. *J. Biol. Chem.* 287, 30385-30394
26. Ravilious, G.E., Westfall, C.S., and Jez, J.M. (2013) Redox-linked gating of nucleotide binding by the N-terminal domain of adenosine 5'-phosphosulfate kinase. *J. Biol. Chem.* 288, 6107-6115
27. Zhang, M., Ravilious, G.E., Hicks, L.M., Jez, J.M., and McCulla, R. (2012) Redox switching of adenosine-5'-phosphosulfate kinase with photoactivatable atomic oxygen precursors. *J. Am. Chem. Soc.* 134, 16979-16982
28. Leustek, T., Murillo, M., and Cervantes, M. (1994) Cloning of a cDNA encoding ATP sulfurylase from *Arabidopsis thaliana* by functional expression in *Saccharomyces cerevisiae*. *Plant Physiol.* 105, 897-902
29. Klonus, D., Höfgen, R., Willmitzer, L., and Riesmeier, J.W. (1994) Isolation and characterization of two cDNA clones encoding ATP-sulfurylases from potato by complementation of a yeast mutant. *Plant J.* 6, 105-112
30. Klonus, D., Riesmeier, J.W., and Willmitzer, L. (1995) A cDNA clone for an ATP-sulfurylase from *Arabidopsis thaliana*. *Plant Physiol.* 107, 653-654
31. Logan, H.M., Cathala, N., Grignon, C., and Davidian, J.C. (1996) Cloning of a cDNA encoded by a member of the *Arabidopsis thaliana* ATP sulfurylase multigene family. *J. Biol. Chem.* 271, 12227-12233
32. Heiss, S., Schäfer, H.J., Haag-Kerwer, A., and Rausch, T. (1999) Cloning sulfur assimilation genes of *Brassica juncea* L.: cadmium differentially affects the expression of a putative low-affinity sulfate transporter and isoforms of ATP sulfurylase and APS reductase. *Plant Mol. Biol.* 39, 847-857
33. Hatzeld, Y., Lee, S., Lee, M., Leustek, T., and Saito, K. (2000) Functional characterization of a gene encoding a fourth ATP sulfurylase isoform from *Arabidopsis thaliana*. *Gene* 248, 51-58
34. Zhu, L., Deng, W.W., Ye, A.H., Yu, M., Wang, Z.X., and Jiang, C.J. (2008) Cloning of two cDNAs encoding a family of ATP sulfurylase from *Camellia sinensis* related to selenium or sulfur metabolism and functional expression in *Escherichia coli*. *Plant Physiol Biochem.* 46, 731-738
35. Renosto, F., Patel, H.C., Martin, R.L., Thomassian, C., Zimmerman, G., and Segel, I.H. (1993) ATP sulfurylase from higher plants: kinetic and structural characterization of the chloroplast and cytosol enzymes from spinach leaf. *Arch. Biochem. Biophys.* 307, 272-285
36. Rotte, C. and Leustek, T. (2000) Differential subcellular localization and expression of ATP sulfurylase and 5'-adenylylsulfate reductase during ontogenesis of *Arabidopsis* leaves indicates that cytosolic and plastid forms of ATP sulfurylase may have specialized functions. *Plant Physiol.* 124, 715-724
37. Brunold, C. and Suter, M. (1984) Regulation of sulfate assimilation by nitrogen nutrition in the duckweed *Lemna minor* L. *Plant Physiol.* 76, 579-583
38. Cacco, G., Saccomani, M., and Ferrari, G. (1997) Development of sulfate uptake capacity and ATP-sulfurylase activity during root elongation in maize. *Plant Physiol.* 60, 582-584
39. Vauclare, P., Kopriva, S., Fell, D., Suter, M., Sticher, L., von Ballmoos, P., Krähenbühl, U., den Camp, R.O., and Brunold, C. (2002) Flux control of sulphate assimilation in *Arabidopsis thaliana*: adenosine 5'-phosphosulphate reductase is more susceptible than ATP sulphurylase to negative control by thiols. *Plant J.* 31, 729-740
40. Liang, G., Yang, F., Yu, D. (2010) MicroRNA395 mediates regulation of sulfate accumulation and allocation in *Arabidopsis thaliana*. *Plant J.* 62, 1046-1057

41. Kawashima, C.G., Matthewman, C.A., Huang, S., Lee, B.R., Yoshimoto, N., Koprivova, A., Rubio-Somoza, I., Todesco, M., Rathjen, T., Saito, K., Takahashi, H., Dalmay, T., and Kopriva, S. (2011) Interplay of SLIM1 and miR395 in the regulation of sulfate assimilation in Arabidopsis. *Plant J.* 66, 863-876
42. Mougous, J.D., Lee, D.H., Hubbard, S.C., Schelle, M.W., Vocadlo, D.J., Berger, J.M., and Bertozzi, C.R. (2006) Molecular basis for G-protein control of the prokaryotic ATP sulfurylase. *Mol. Cell* 21, 109-122
43. Beynon, J.D., MacRae I.J., Huston, S.L., Nelson, D.C., Segel, I.H., and Fisher, A.J. (2001) Crystal structure of ATP sulfurylase from the bacterial symbiont of the hydrothermal vent tubeworm *Riftia pachyptila*. *Biochemistry* 40, 14509-14517
44. Taguchi, Y., Sugishima, M., and Fukuyama, K. (2004) Crystal structure of a novel zinc-binding ATP sulfurylase from *Thermus thermophilus* HB8. *Biochemistry* 43, 4111-4118
45. Yu, Z., Lansdon, E.B., Segel, I.H., and Fisher, A.J. (2007) Crystal structure of the biofunctional ATP sulfurylase-APS kinase from the chemolithotrophic thermophile *Aquifex aeolicus*. *J. Mol. Biol.* 365, 732-743
46. Parey, K., Demmer, U., Warkentin, E., Wynen, A., Ermler, U., and Dahl, C. (2013) Structural, biochemical, and genetic characterization of dissimilatory ATP sulfurylase from *Allochrochromatium vinosum*. *PLoS One* 8, e74707
47. Ullrich, T.C., Blaesse, M., and Huber, R. (2001) Crystal structure of ATP sulfurylase from *Saccharomyces cerevisiae*, a key enzyme in sulfate activation. *EMBO J.* 20, 316-329
48. Ullrich, T.C. and Huber, R. (2001) The complex structures of ATP sulfurylase with thiosulfate, ADP, and chlorate reveal new insights in inhibitory effects and the catalytic cycle. *J. Mol. Biol.* 313, 1117-1125
49. MacRae, I., Segel, I.H., and Fisher, A.J. (2001) Crystal structure of ATP sulfurylase from *Penicillium chrysogenum*: insights into the allosteric regulation of sulfate assimilation. *Biochemistry* 40, 6795-6804
50. MacRae, I., Segel, I.H., and Fisher, A.J. (2002) Allosteric inhibition via R-state destabilization in ATP sulfurylase from *Penicillium chrysogenum*. *Nature Struct. Biol.* 9, 945-949
51. Harjes, S., Bayer, P., and Scheidig, A.J. (2005) The crystal structure of human PAPS synthetase 1 reveals asymmetry in substrate binding. *J. Mol. Biol.* 347, 623-635
52. Ravilious, G.E., Herrmann, J., Lee, S.G., Westfall, C.S., and Jez, J.M. (2013) Kinetic mechanism of a dimeric ATP sulfurylase from plants. *Biosci. Rep.* 33, e00053
53. Otwinowski, Z. and Minor, W. (1997) Processing of x-ray diffraction data collected in oscillation mode. *Methods Enzymol.* 276, 307-326
54. McCoy, A.J., Grosse-Kunstleve, R.W., Adams, P.D., Winn, M.D., Storoni, L.C., and Read, R.J. (2007) Phaser crystallographic software. *J. Appl. Cryst.* 40, 658-674
55. Emsley, P., Lohkamp, B., Scott, W.G., and Cowtan, K. (2010) Features and development of Coot. *Acta Cryst. D* 66, 486-501
56. Adams, P.D., Afonine, P.V., Bunkóczi, G., Chen, V.B., Davis, I.W., Echols, N., Headd, J.J., Hung, L.W., Kapral, G.J., Grosse-Kunstleve, R.W., McCoy, A.J., Moriarty, N.W., Oeffner, R., Read, R.J., Richardson, D.C., Richardson, J.S., Terwilliger, T.C., and Zwart, P.H. (2010) PHENIX: a comprehensive Python-based system for macromolecular structure solution. *Acta Cryst. D* 66, 213-221
57. Trott, O. and Olson, A.J. (2010) AutoDock Vina: improving the speed and accuracy of docking with a new scoring function, efficient optimization, and multithreading. *J. Comput. Chem.* 31, 455-461
58. Holm, L. and Rosenström, P. (2010) Dali server: conservation mapping in 3D. *Nucl. Acids Res.* 38, W545-549
59. Koprivova, A., Giovannetti, M., Baraniecka, P., Lee, B.R., Grondin, C., Loudet, O., and Kopriva, S. (2013) Natural variation in the ATPS1 isoform of ATP sulfurylase contributes to the control of sulfate levels in Arabidopsis. *Plant Physiol.* 163, 1133-1141.

60. Gan, X., Stegle, O., Behr, J., Steffen, J.G., Drewe, P., Hildebrand, K.L., Lyngsoe, R., Schultheiss, S.J., Osborne, E.J., Sreedharan, V.T., Kahles, A., Bohnert, R., Jean, G., Derwent, P., Kersey, P., Belfield, E.J., Harberd, N.P., Kemen, E., Toomajian, C., Kover, P.X., Clark, R.M., Rättsch, G., and Mott, R. (2011) Multiple reference genomes and transcriptomes for *Arabidopsis thaliana*. *Nature* 477, 419-423
61. Phartiyal, P., Kim, W.S., Cahoon, R.E., Jez, J.M., and Krishnan, H.B. (2008) The role 5'-adenylylsulfate reductase in the sulfur assimilation pathway of soybean: molecular cloning, kinetic characterization, and gene expression. *Phytochemistry* 69, 356-364
62. Bradley, M.E., Rest, J.S., Li, W.H., and Schwartz, N.B. (2009) Sulfate activation enzymes: phylogeny and association with pyrophosphatase. *J. Mol. Evol.* 68, 1-13
63. Deyrup, A.T., Singh, B., Krishnan, S., Lyle, S., and Schwartz, N.B. (1999) Chemical modification and site-directed mutagenesis of conserved HXXH and PP-loop motif arginines and histidines in the murine bifunctional ATP sulfurylase/adenosine 5'-phosphosulfate kinase. *J. Biol. Chem.* 274, 28929-28936
64. Venkatachalam, K.V., Fuda, H., Koonin, E.V., and Strott, C.A. (1999) Site-selected mutagenesis of a conserved nucleotide binding HXGH motif located in the ATP sulfurylase domain of human bifunctional 3'-phosphoadenosine 5'-phosphosulfate synthase. *J. Biol. Chem.* 274, 2601-2604
65. Perona, J.J., Rould, M.A., and Steitz, T.A. (1993) Structural basis for transfer RNA aminoacylation by *Escherichia coli* glutaminyl-tRNA synthetase. *Biochemistry* 32, 8758-8771
66. Park, Y.S., Gee, P., Sanker, S., Schurter, E.J., Zuiderweg, E.R., and Kent, C. (1997) Identification of functional conserved residues of CTP:glycerol-3-phosphate cytidylyltransferase: role of histidines in the conserved HXGH in catalysis. *J. Biol. Chem.* 272, 15161-15166
67. Weber, C.H., Park, Y.S., Sanker, S., Kent, C., and Ludwig, M.L. (1999) A prototypical cytidylyltransferase: CTP:glycerol-3-phosphate cytidylyltransferase from *Bacillus subtilis*. *Structure* 7, 1113-1124
68. Parey, K., Fritz, G., Ermler, U., and Kroneck, P.M. (2013) Conserving energy with sulfate around 100 °C - structure and mechanism of key metal enzymes in hyperthermophilic *Archaeoglobus fulgidus*. *Metallomics* 5, 302-317
69. Corpet, F. (1988) Multiple sequence alignment with hierarchical clustering. *Nucl. Acids Res.* 16, 10881-10890

FOOTNOTES

*This work was supported by funds from the National Science Foundation (MCB-0904215). J.H. and S.E.M. were supported by an American Society of Plant Biologists Summer Undergraduate Research Fellowship and the Washington University Summer Scholars in Biology and Biomedical Research Program, respectively. C.S.W. was supported by a U.S. Department of Agriculture National Institute of Food and Agriculture pre-doctoral fellowship [MOW-2010-05240]. Portions of this research were carried out at the Argonne National Laboratory Structural Biology Center of the Advanced Photon Source, a national user facility operated by the University of Chicago for the Department of Energy Office of Biological and Environmental Research (DE-AC02-06CH11357). Product names are necessary to report factually on available data; however, the USDA neither guarantees nor warrants the standard of product, and the use of the name by the USDA implies no approval of the product to the exclusion of others that may be suitable.

⁵To whom correspondence should be addressed: Department of Biology, Washington University, One Brookings Drive, Campus Box 1137, St. Louis, MO 63130. Phone: 314-935-3376; E-mail: jjez@biology2.wustl.edu.

⁶Abbreviations are: APS, adenosine-5'-phosphosulfate; APSK, adenosine-5'-phosphosulfate kinase, also known as adenylyl-sulfate kinase, E.C. 2.7.1.25; ATP sulfurylase, ATP:sulfate adenylyltransferase, E.C. 2.7.7.4; GmATPS, *Glycine max* (soybean) ATP sulfurylase; PAPS, 3'-phosphoadenosine-5'-phosphosulfate; PP_i, pyrophosphate.

Table 1. Summary of crystallographic statistics for the GmATPS•APS complex.

<u>Crystal</u>	
Space group	C222
Cell dimensions	$a = 204.3 \text{ \AA}$, $b = 230.8 \text{ \AA}$, $c = 159.2 \text{ \AA}$
<u>Data Collection</u>	
Wavelength (\AA)	0.979
Resolution range (\AA) (highest shell resolution)	48.2 - 2.48 (2.52 - 2.48)
Reflections (total/unique)	686,045 / 123,420
Completeness (highest shell)	93.6% (93.7%)
$\langle I/\sigma \rangle$ (highest shell)	18.0 (2.5)
R_{sym}^a (highest shell)	9.4% (51.5%)
<u>Model and Refinement</u>	
$R_{\text{cryst}}^b / R_{\text{free}}^c$	17.0 / 21.8
No. of protein atoms	25,454
No. of water molecules	825
No. of ligand atoms	216
R.m.s. deviation, bond lengths (\AA)	0.008
R.m.s. deviation, bond angles ($^\circ$)	1.149
Avg. B-factor (\AA^2) - protein, waters, ligands	49.4, 43.7, 37.7
Stereochemistry: most favored, allowed, outlier	97.8, 2.1, 0.1%
^a $R_{\text{sym}} = \sum I_h - \langle I_h \rangle / \sum I_h$, where $\langle I_h \rangle$ is the average intensity over symmetry. ^b $R_{\text{cryst}} = \sum F_o - \langle F_c \rangle / \sum F_o$, where summation is over the data used for refinement. ^c R_{free} is defined the same as R_{cryst} , but was calculated using 5% of data excluded from refinement.	

Table 2. Steady-state kinetic parameters of wild-type and mutant GmATPS for APS synthesis.

protein	V/E (s^{-1})	K_m^{ATP} (μM)	V/K_m^{ATP} ($M^{-1} s^{-1}$)	$K_m^{sulfate}$ (μM)	$V/K_m^{sulfate}$ ($M^{-1} s^{-1}$)
wild-type	0.512 ± 0.013	165 ± 18	3,100	320 ± 25	1,600
F245L	0.283 ± 0.022	$2,150 \pm 338$	132	306 ± 52	93
Q246N	0.134 ± 0.007	880 ± 145	155	236 ± 57	579
Q246A	0.288 ± 0.010	346 ± 30	833	$1,070 \pm 103$	269
H333Q	0.162 ± 0.005	575 ± 51	281	311 ± 53	520

Reactions were performed as described under “Experimental Procedures.” All parameters are expressed as a mean \pm S.E. for an $n = 3$.

Table 3. Steady-state kinetic parameters of wild-type and mutant GmATPS for ATP synthesis.

protein	V/E (s^{-1})	K_m^{APS} (μM)	V/K_m^{APS} ($M^{-1} s^{-1}$)	K_m^{PPi} (μM)	V/K_m^{PPi} ($M^{-1} s^{-1}$)
wild-type	32.0 ± 1.4	34.2 ± 5.2	936,000	45.8 ± 6.8	699,000
F245L	93.8 ± 6.1	24.7 ± 5.8	3,798,000	118 ± 29	795,000
F245A	108 ± 9	36.3 ± 5.6	2,980,000	153 ± 24	706,000
Q246E	10.3 ± 1.7	312 ± 26	33,000	61.1 ± 3.9	170,000
Q246N	60.6 ± 1.8	45.0 ± 5.4	1,350,000	55.6 ± 6.1	1,090,000
Q246A	64.3 ± 4.1	40.2 ± 8.5	1,600,000	117 ± 25	373,000
R248K	19.7 ± 1.4	47.0 ± 4.6	419,000	428 ± 78	46,000
N249D	0.104 ± 0.005	6.51 ± 1.79	16,000	69.4 ± 14.1	1,500
N249A	34.6 ± 4.3	43.2 ± 6.1	801,000	$1,078 \pm 153$	32,100
H252N	40.3 ± 2.5	27.2 ± 4.4	1,480,000	85.0 ± 17.2	474,000
H255Q	63.5 ± 2.8	22.6 ± 2.2	2,810,000	114 ± 12	557,000
H255A	2.45 ± 0.16	4.41 ± 0.55	556,000	39.9 ± 6.2	61,900
L258V	129 ± 8	38.5 ± 5.4	3,350,000	208 ± 26	629,000
L258A	109 ± 5	28.2 ± 2.9	3,870,000	373 ± 34	292,000
H333Q	27.0 ± 1.6	12.7 ± 2.6	2,130,000	22.0 ± 3.0	1,130,000
R349K	3.22 ± 0.11	34.6 ± 6.7	93,100	590 ± 96	5,460

Reactions were performed as described under “Experimental Procedures.” All parameters are expressed as a mean \pm S.E. for an $n = 3$.

Table 4. Summary of variation in *Arabidopsis* ATPS1 haplotypes and the ATPS activities and sulfate contents of representative accessions.

mutation	comment	number of accessions	example accession	sulfate content ($\mu\text{mol/g DW}$)	ATPS activity (nmol/min/mg protein)
wild-type	<i>A. thaliana</i> Col-0	-	Col-0	7.6 ± 1.4	145 ± 23
<i>atps1</i>	<i>atps1 A. thaliana</i> Col-0	-	<i>atps1</i>	16 ± 2	92 ± 19
S9R	transit peptide	14	Tsu-0	8 ± 1	n.d.
V43N	transit peptide	5	Dog-4	11.5 ± 2.0 *	140 ± 40
G56S	invariant in <i>A. thaliana</i> Col-0; disordered region	11	UII2-3	8.2 ± 2	121 ± 10
L122V	invariant in <i>A. thaliana</i> Col-0; dimer interface	1	Vie-0	14 ± 1	135 ± 10
T150S	loop region	36	Ang-0	4.6 ± 0.3 *	n.d.
A144T/T150S	loop region	2	TDr-2	n.a	n.a.
N160K	loop region	14	Kn-0	7 ± 0.5	n.d.
S166N	Asn in other <i>A. thaliana</i> isoforms	8	Edu-1	n.a	n.a
E169A	invariant in <i>A. thaliana</i> Col-0; dimer interface	6	Goettingen-7	11.3 ± 0.8 *	135 ± 40
T198A	invariant in <i>A. thaliana</i> Col-0; internal packing	2	Ciste-2	11.1 ± 2.2 *	140 ± 36
N202S ^a	loop region	1	Hov3-2	n.a	n.a
E312V	loop region	1	Sakata	n.a	n.a
V316F	internal packing	1	T800	9.9 ± 2.1	247 ± 11 *
A337S	invariant in <i>A. thaliana</i> Col-0; loop region	18	Bil-7	7.6 ± 0.1	145 ± 51
G342D	invariant in <i>A. thaliana</i> Col-0; internal packing	1	Naes-2	12.3 ± 3 *	72 ± 3 *
K372R	Arg in other <i>A. thaliana</i> isoforms; dimer interface	1	Kulturen	10.7 ± 1.6 *	n.d.

The haplotype information is derived from 1001 Genomes Browser. ATP sulfurylase activity and sulfate levels were determined in leaves of accessions representative of each haplotype grown for 5 weeks in controlled environment room under short days. For comparison, ATP sulfurylase activity and sulfate were measured in *A. thaliana* Col-0 and *atps1* mutant grown at the same conditions. Asterisks mark values significantly ($P < 0.05$) different from wild-type. n.d., activity not determined, n.a. accession not available or not germinated. ^aThe sequence quality is low in this region; the haplotype might be a sequencing error.

FIGURE LEGENDS

Figure 1. ATP sulfurylase domain structure and oligomerization. (A) Overall reaction catalyzed by ATP sulfurylase. (B) Dendrogram of ATP sulfurylase sequences from a bacterial symbiont of hydrothermal vent tubeworm *Riftia pachyptila* (RpsATPS), soybean (*Glycine max*: GmATPS), human (HsAPSK/ATPS or PAPS synthetase), *Thermus thermophilus* (TtATPS), *Aquifex aeolicus* (AaATPS/APSK), *Penicillium chrysogenum* (PcATPS), *Saccharomyces cerevisiae* (ScATPS), and *Pseudomonas syringae* (PsATPS). The dendrogram was generated from multiple sequence alignment of ATP sulfurylases using the MultAlin webpage (69). (C) The domain structure of each protein is shown with regions corresponding to ATP sulfurylase, APS kinase, APS kinase-like, and GTPase colored purple, yellow, green, and light blue, respectively.

Figure 2. Three-dimensional structure of GmATPS. (A) Ribbon diagram showing the structure of the GmATPS monomer. The N- and C-termini residues are indicated. The α -helices and β -strands are colored blue and gold, respectively, and are numbered. APS bound in the active site is shown as a space-filling model. In this orientation, the N-terminal domain corresponds to the lower half of the structure and the C-terminal domain corresponds to the upper half of the structure. All structural figures were generated using PyMOL (PyMOL Molecular Graphics System, Version 1.5.0.4 Schrödinger, LLC). (B) Overall structure of the GmATPS dimer. Structural features in one monomer are colored as in panel A with α -helices and β -strands of the second monomer colored green and rose, respectively. Secondary structure features along the dimer interface are indicated. The position of bound APS in each monomer is shown by the space-filling model.

Figure 3. Sequence comparison of ATP sulfurylases. A multiple sequence alignment of the ATP sulfurylases from soybean (GmATPS; AF452454) human (HsPAPPS; O43252), the *Riftia* symbiont (RpsATPS; Q54506), *S. cerevisiae* (ScATPS, P08563), *P. chrysogenum* (PcATPS, Q12650), *A. aeolicus* (AaATPS, O67174), and *T. thermophilus* (TtATPS, Q5SKH7) is shown with amino acid numbering indicated in parenthesis. The α -helices (blue rectangles) and β -strands (yellow rectangles) of GmATPS are depicted over the alignment. Conserved residues are highlighted in orange with residues in white indicating a variation from the conserved sequence. Red highlight denotes active site residues in GmATPS. The linker region between the N- and C-terminal structural domains is indicated. The light grey boxes indicate regions at the dimer interface of GmATPS; these regions also display large sequence variation across the ATP sulfurylases. Multiple sequence alignment used the MultAlin webpage (70).

Figure 4. Structural diversity in ATP sulfurylases. The three-dimensional structures of the dimeric monofunctional ATP sulfurylases from soybean (GmATPS; described here), the *Riftia* symbiont (RpsATPS), and *T. thermophilus* (TtATPS); the dimeric bifunctional PAPS synthetases from human (HsAPSK/ATPS) and *A. aeolicus* (AaATPS/APSK); the heterodimeric monofunctional ATP sulfurylase from *P. syringae* (PsATPS); and the homohexameric enzyme from fungi (PcATPS) are shown as ribbon diagrams. The domain structure of each protein is colored by function as follows: ATP sulfurylase - rose; APS kinase - yellow; APS kinase-like - green; and GTPase - blue.

Figure 5. Active site of the GmATPS•APS complex. (A) Electron density of APS in the GmATPS active site. A final $F_o - F_c$ omit map (1.5σ) is shown. (B) Stereo-view molecular surface rendering of the GmATPS active site. The view is oriented down the putative pyrophosphate binding site. Surfaces corresponding to Arg248 and Arg349 are colored (blue). APS is shown as a stick model. (C) Stereo-view showing protein-ligand interactions in the GmATPS•APS complex. Dotted lines represent hydrogen bonds between active site residues and the ligand.

Figure 6. Active site models for the forward and reverse reactions catalyzed by GmATPS. (A) Model of substrates of the forward reaction in the GmATPS active site. ATP adopts a U-shaped conformation that allows nucleophilic attack by the sulfate ion. **(B)** Model of substrates of the reverse reaction in the GmATPS active site. The position of APS is from the GmATPS•APS x-ray crystal structure and PP_i was computationally docked in the active site.

Figure 7. Structural mapping of *Arabidopsis thaliana* haplotype differences in ATP sulfurylase. Positions of mutations in *Arabidopsis* ATPS1 haplotypes were mapped to the corresponding residues of GmATPS. Residues of each monomer are colored as red and blue space-filling models, respectively. The position of APS in the structure is shown as the gold space-filling model. The orientation shown is the same as in Figure 2B.

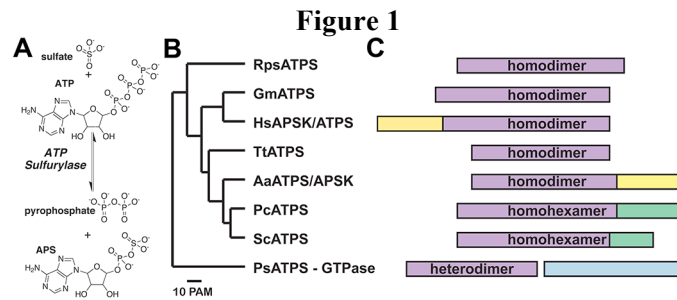


Figure 2

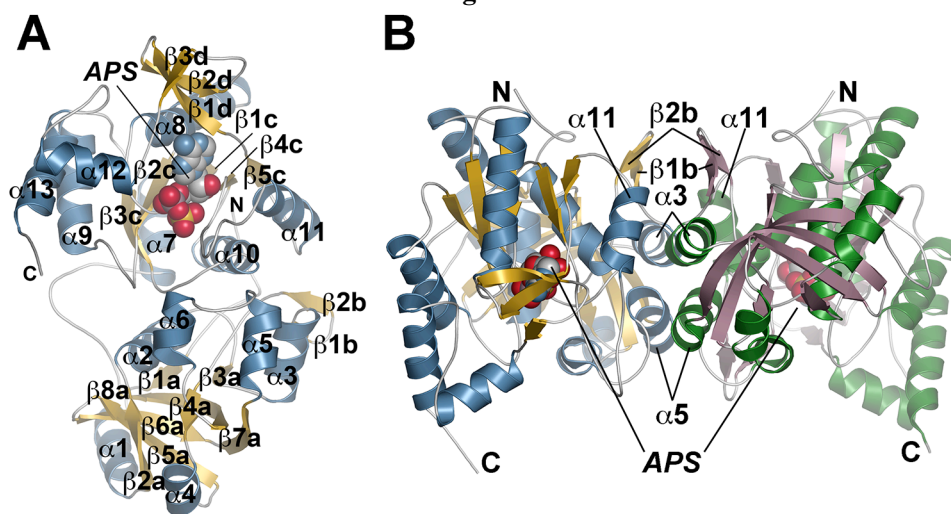
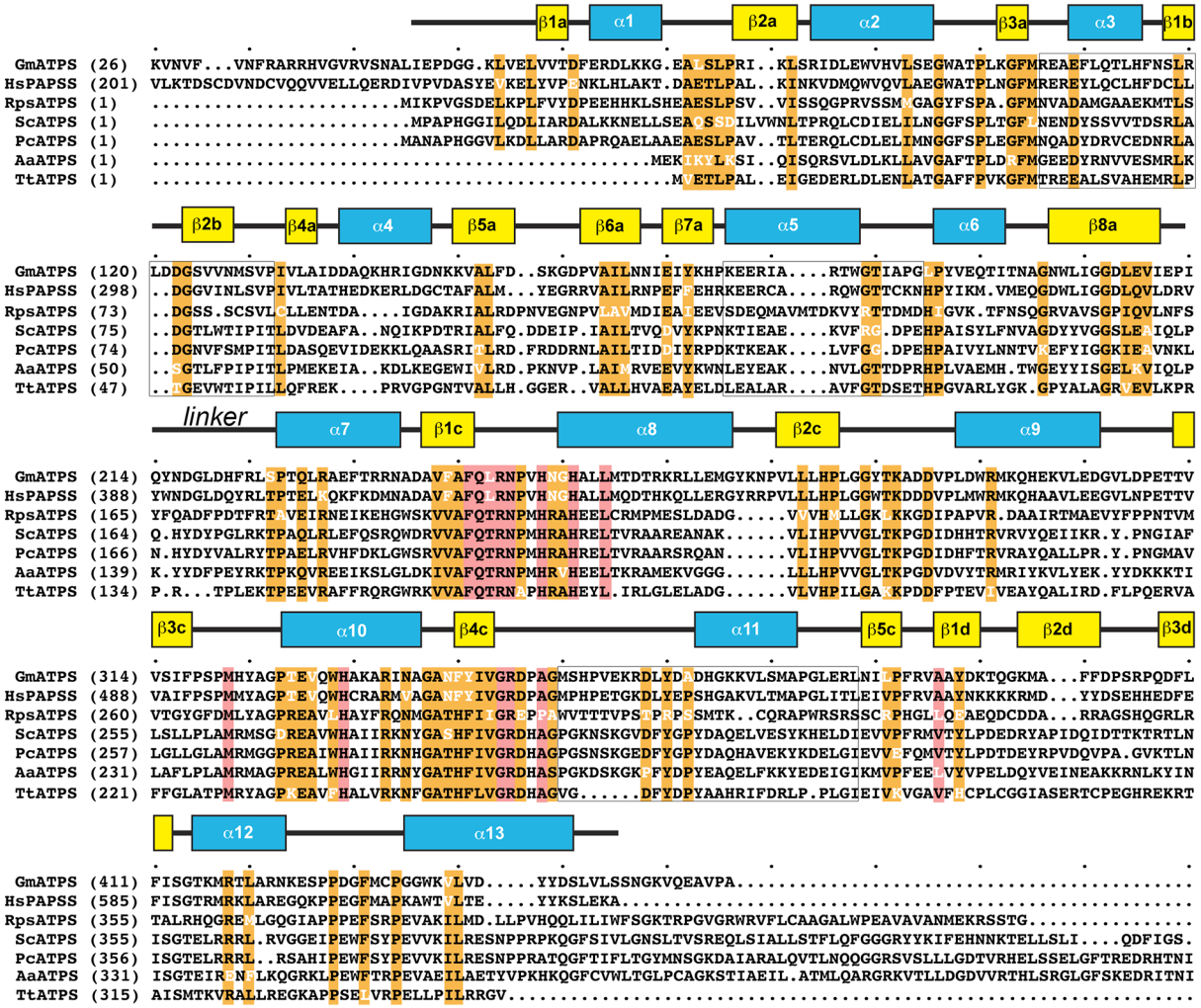
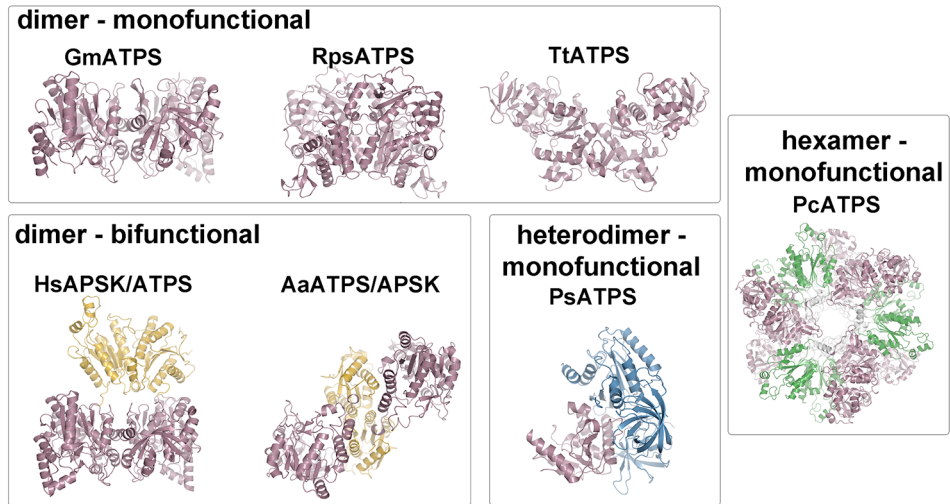


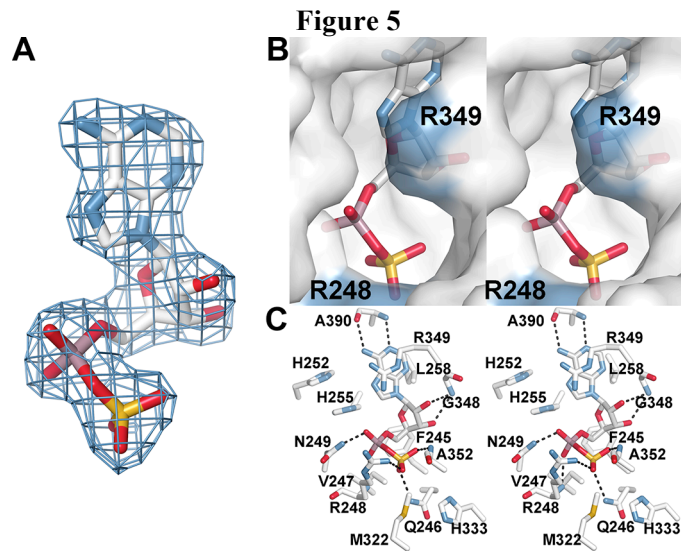
Figure 3



Confidential

Figure 4





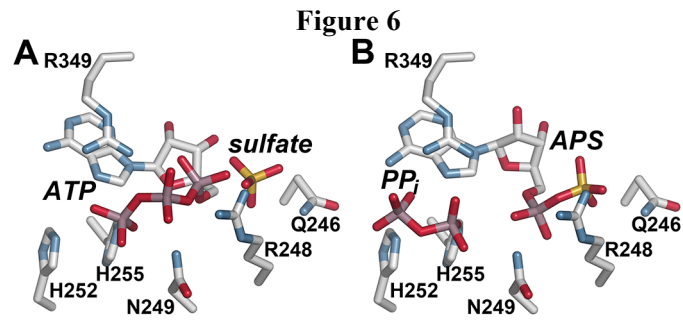


Figure 7

